Supplementary Information

Su et al.

Materials and Methods

Molecular cloning

The *msrE* gene with its putative promoter was amplified from *P. aeruginosa* PASGNDM699 genome (GenBank accession no. CP020704) and ligated into pUC18 vector. The sequence corresponding to full-length MsrE was cloned from the pUCP18::*msrE* plasmid and ligated into pET22b vector (Novagen) introducing the T7 promoter, N-terminal His_6-tag, and ampicillin resistance gene for selection. Site-directed mutagenesis (1) was used to introduce mutations to *msrE* gene. For construction of pJN105-P_{BAD}-*msrE* plasmid, the native and mutant *msrE* genes were cloned from the expression vector using primers EcoRI-RBS-*msrE* (CGGAATTCTTAACTTTAAGGAGGAGATATAATGAGTTTAATTATTAAAG) and XbaI-*msrE* (GCTCTAGATTAACAATCTCTCTCAAAAGTCT). The PCR product was digested with EcoRI and XbaI and inserted into the corresponding sites of pJN105 vector to yield a pJN105-P_{BAD}-*msrE*, for which the expression of *msrE* is under the control of the arabinose inducible promoter P_{BAD}. The pJN105-P_{BAD}-*ettA*-EQ2 plasmid was constructed in the same manner, except that the insert was amplified from expression plasmid pDBHT-2-Tev-EQ2 with primers EcoRI-RBS-*ettA* (CGGAATTCTTAACTTTAAGGAGGAGATATAATGGCTCAATTCGTTTATACC) and XbaI-*ettA* (GCTCTAGATTACTTCGCAATACGCTTGT). The plasmids were transformed into *E. coli* K12 MG1655 strain by heat shock, after which the

transformants were selected on LB agar plates supplemented with 30 μg/ml gentamicin.

MIC assay and growth curve

The AZM MIC of each strain was determined in a 96-well plate by broth micro-dilution according to CLSI (Clinical and Laboratory Standards Institute) guidelines. Growth of bacteria as indicated by optical density at 600 nm (OD_{600}) was detected by a microplate reader (TECAN) after incubation at 37 ˚C for 16 hours. The growth curve experiment was performed in a 24-well plate. *E. coli* K12 MG1655 strains were grown in LB medium in the presence of either 0.2% glucose or 0.2% arabinose, to inhibit or induce the expression of *msrE*, respectively, and incubated at 37 ˚C with 200 rpm shaking. OD_{600} of the bacterial culture was monitored by a microplate reader (TECAN). Four replicates were performed for each growth curve experiment and mean ± standard deviations were shown in the figures.

MsrE protein purification

MsrE expression constructs were transformed into *E. coli* BL21 (DE3) (Novagen) chemo-competent cells and grown in 5 L of 2xYT broth at 37 °C until OD_{600} reached 0.6. Protein expression was induced with 0.5 mM of IPTG and carried out at 16 °C for 18 hours (200 rpm). Cells were harvested by centrifugation at 4 °C, 4,000 g for 20 min; re-suspended in lysis buffer (50 mM sodium phosphate buffer pH 8, 300 mM NaCl, 10% glycerol, 5 mM 2-mercaptoethanol, and 7 mM phenylmethane sulfonyl fluoride). All the following steps were carried out on ice or at 4 °C unless otherwise stated. Cell lysis was performed using Microfluidizer LM20 (Microfluidics) at 20,000 psi. Lysate was clarified by centrifugation at 22,000 g for 40 min and supernatant was filtered through 0.45 μm Sterivex filters (Millipore). MsrE variants were purified using three chromatographic steps and the AKTA Express protein purification system

(GE Healthcare). Briefly, 5 ml HisTrap FF column (GE Healthcare) nickel affinity chromatography was followed by 5 ml HiTrap Q FF column (GE Healthcare) ion exchange chromatography, and HiLoad 16/60 Superdex 200 column (GE Healthcare) size exclusion chromatography. Purified proteins (in 25 mM Tris-HCl pH 8 and 150 mM NaCl) were concentrated using 30 kDa cut-off filters (Millipore), snap-frozen in liquid nitrogen, and stored at −80 °C.

In vitro transcription/translation assays

E. coli S30 extract system for circular DNA was used (Promega). Briefly, 5 µl of S30 extract was added to a 20 µl reaction mixture containing 0.1 mM amino acids, 10 µl S30 premix, 1 µg of pBEST*luc*™ DNA template, 10 µM AZM, and purified MsrE proteins as indicated. Samples were incubated for 1 hour at 37 °C followed by 5 min inactivation on ice. The level of transcription/translation was quantified by monitoring the expression of luciferase by the addition of luciferase assay reagent (Promega) and the measurement of luminescence using Tecan Spark 10M.

Ribosome preparation and MsrE-ribosome-AZM binding assay

Thermus thermophilus 70S ribosomes were purified as described previously (2). The purified ribosomes (f.c. 5 µM) and full-length MsrE protein (f.c. 25 µM) were pre-incubated with AZM (f.c. 250 µM) and AMP-PNP or ATP (f.c. 100 µM), respectively, in Buffer G (5 mM HEPES-KOH pH 7.5, 50 mM KCl, 10 mM NH_4Cl, 10 mM MgOAc, and 6 mM 2-mercaptoethanol) at room temperature (RT) for 30 min. Ribosome and MsrE samples were mixed and incubated at RT for additional 30 min. For control, ribosomes (pre-incubated in the presence and absence of AZM) were also analysed. Samples (final volume 50 µl) were filtered using Spin-X 0.22 µm filters, applied onto 100 µl 1.1 M sucrose cushion in Buffer G, and ultra-centrifuged at 4 °C and 100,000 rpm for 3 hours (Beckman TLA 100 rotor). Pellets were washed twice

and re-suspended in Buffer G. Aliquots were analysed on NuPAGE 4-12% Bis-Tris Gels (Invitrogen), MOPS electrophoresis buffer and SYPRO Ruby (BioRad) for quantitative staining.

Mass Spectrometry

Ribosome pellets (following ultra-centrifugation through sucrose cushion) were washed thrice and re-suspended in 50 µl MilliQ water. Samples were heat-treated at 86 °C for 5 min to release AZM from ribosome and placed on ice. Ethanol (f.c. 80%) was added, samples were centrifuged for 10 min at 15,000 rpm, divided into four parallels, and evaporated to dryness in a Concentrator Plus speed-vac (Eppendorf). One parallel was used for NuPAGE and SYPRO Ruby staining to quantify r-proteins and bound MsrE. Three parallels were reconstituted for LC-MS analysis by vortexing for 30 min in 5 µl of 50% acetonitrile (ACN) containing 0.1% formic acid (FA), after which 15 µl of 0.1% FA was added to bring the final volume to 20 µl. LC-MS analysis was performed on an LTQ FT Ultra Mass Spectrometer (Thermo Fisher Scientific) coupled to a Vanquish UHPLC System (Thermo Fisher Scientific). Samples were resolved on a ZORBAX RRHD Eclipse Plus C18 column (Agilent; 2.1 x 100 mm, 1.8 µm particle size) with Buffer A comprising of 0.1% FA in HPLC water and Buffer B containing 0.1% FA in 100% ACN using the following 30 min gradient: 18 min 20–60% B, 1 min 60–90% B, and 2 min 90% B, 0.1 min 90–20%, 9 min 20% B. The flow rate of mobile phase was set at 0.05 ml/min for 18 min, followed by 0.2 ml/min for 12 min. Data was acquired using XCalibur software and the FTMS was set in positive mode with scan range set to between 300 and 800 m/z at a resolution of 100,000. The amount of AZM in each sample was determined by area under the curve analysis of the extract ion chromatogram (XIC) in +/- 5ppm range from the 2+ ions at m/z 375.262 using an in-house program.

Complex formation, cryo-EM data acquisition, and processing

For cryo-EM grid preparation, the MsrE-ribosome complex was reconstituted in Buffer G in the following manner. First, 0.24 μM ribosomes were incubated with 0.48 μM of mRNA Z4C at 55 °C for 30 min as described in (3). Ribosome-mRNA incubation was followed by incubation with 0.48 μM $tRNA^{fMet}$ at 55 °C for 30 min. In parallel, 12 μM MsrE was incubated with 100 μM of AMP-PNP at room temperature for 30 min. Finally, the ribosome and MsrE reaction mixtures were combined and allowed to form a complex at 37 °C for 30 min. and kept on ice.

4.4 μl aliquots of the reconstituted MsrE-ribosome complex were incubated on a glow-discharged 2-nm carbon-coated holey grid (Quantifoil R2/2) for 20 sec. The grids were blotted for 2.5 sec. (15 sec. wait time and with a force of 1 once for 1 sample grid) in 100% humidity at 4 °C and flash-frozen in liquid N_2-cooled liquid ethane using FEI Vitrobot. Grids were loaded onto FEI Titan Krios cryo-transmission electron microscope operated at 300 kV (CBIS, DBS, NUS Singapore). Data was acquired automatically using Leginon software (4). Image acquisition was performed in movie mode as sets of 20 frames (total dose of 50 electrons per $Å^2$) at a nominal magnification of 75,000X, resulting in a pixel size of 1.1 Å over defocus values of -1.5 to -2.5 μm.

A total of 6,888 micrographs were selected for data processing. Whole-image drift correction and CTF parameter estimation were performed using programs Unblur (5) and CTFFIND4 (6), respectively. Particles picking and data processing was done in Relion 2.0 (7, 8). A total of 310,270 auto-picked particles were then subjected to reference-free 2D classification to remove the non-ribosome particles. After two rounds of 2D classification, 186,654 selected particles were used for 3D classification using 60Å filtered empty 70S ribosome as a reference to sort out the heterogeneity.

Finally, 127,778 particles with strong density for MsrE and P-tRNA were utilized for final reconstruction with statistical movie processing to correct beam induced particle movements in Relion (7, 8). Final reconstruction yielded a map of 3.6 Å resolution, as determined with the gold standard Fourier cell correlation (FCS) criteria in Relion (Fig. S4). The MsrE model was built in RaptorX web server (9) using sequence from *P. aeruginosa* PASGNDM699. Initial docking of 50S, 30S, tRNA (PDB ID: 5AA0) structures and MsrE model into cryo-EM maps was performed in Chimera (10). Structures were subsequently rigid fitted manually and refined in both Coot (11) and Phenix (12). Local resolution estimation was performed using ResMap (13). All the figures reported in the manuscript are prepared in PyMol unless otherwise stated.

Supplementary Figures

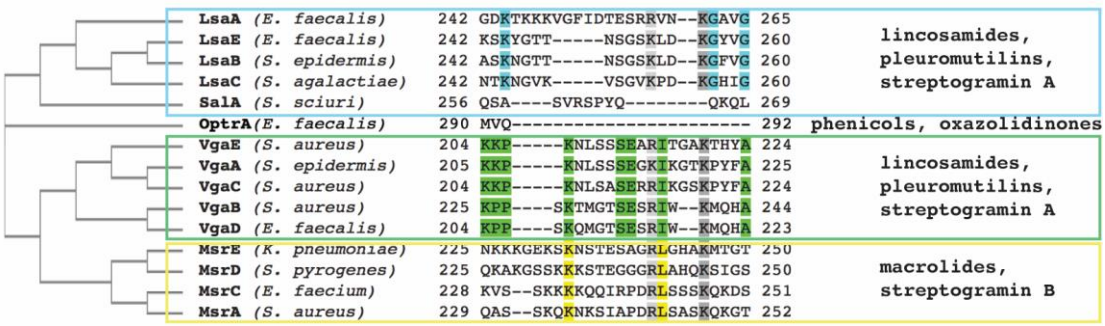

Figure S1. Antibiotic resistance ATP-binding cassette family F phylogeny (left), alignment of the domain linker extended loop residues (middle), and corresponding antibiotic resistance profiles (right). Conserved and semi-conserved residues are shown in dark and light grey, respectively. Residues conserved in Lsa (blue), Vga (green), and Msr (yellow) members are also highlighted.

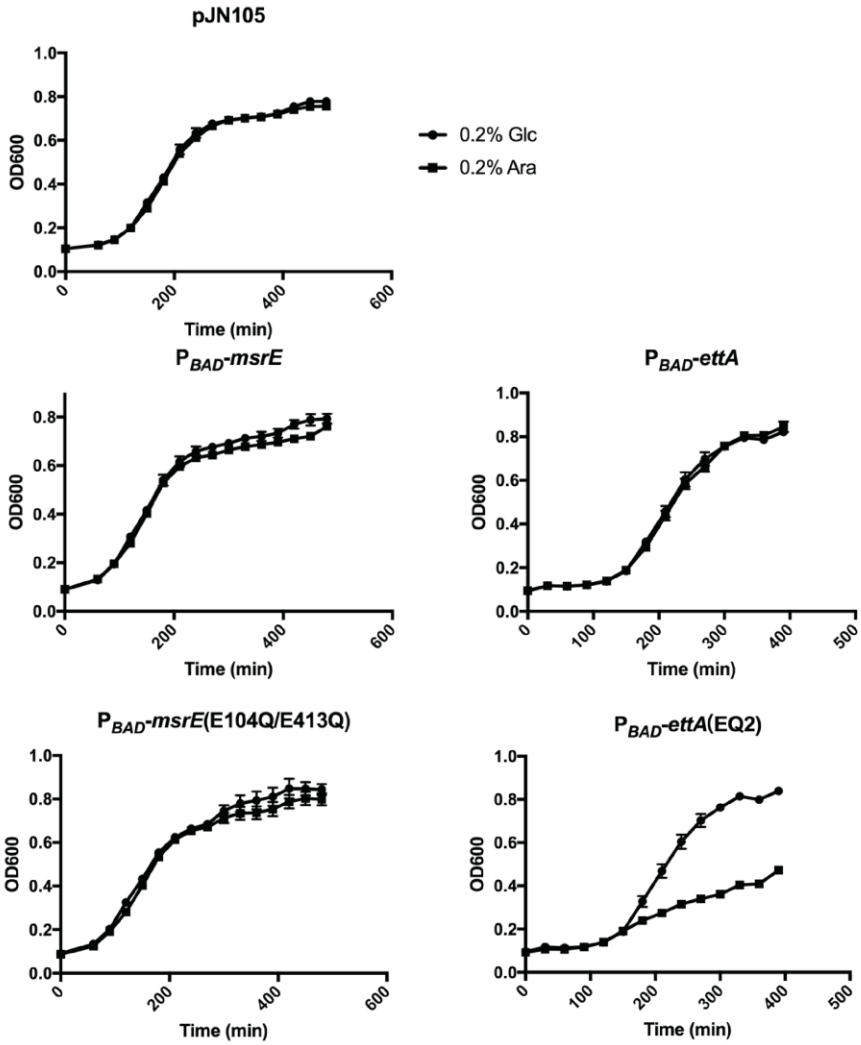

Figure S2. Effect of MsrE expression on *E. coli* growth. *E. coli* K12 MG1655 strain was transformed with pJN105 plasmid carrying native or ATP-hydrolysis deficient MsrE (left) or EttA (right) proteins under the control of arabinose inducible promoter P_{BAD}. Protein expression was either induced with 0.2% arabinose or repressed with 0.2% glucose. Empty pJN105 plasmid was used as control. For proof of concept, the growth curve of MG1655/pJN105-ettA(EQ2) showed repressed growth in the presence of 0.2% arabinose, which is consistent with the observation by Boël et al. (14). The EttA EQ2 mutant (E188Q/E470Q) corresponds to MsrE(E104Q/E413Q) mutant. Induction of MsrE or MsrE(E104Q/E413Q) did not significantly affect the growth curve of MG1655 strain.

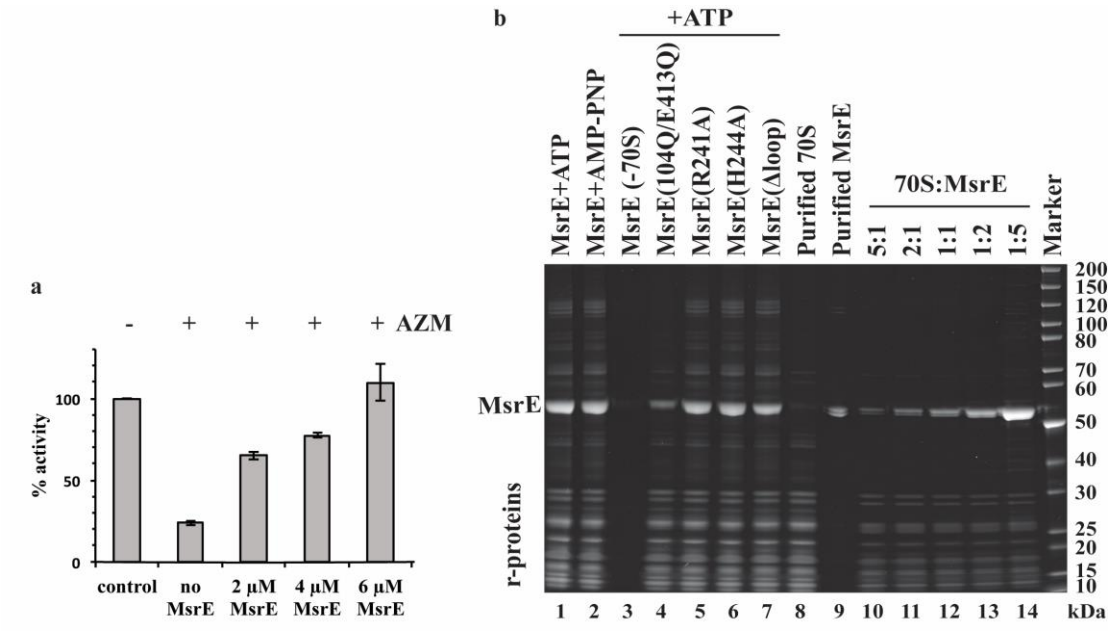

Figure S3. MsrE effect *in vitro* transcription/translation inhibited by AZM and ribosome binding stoichiometry. (a) MsrE rescues *E. coli in vitro* transcription/translation from AZM inhibition in dose-dependent manner. First column is untreated conditions, for rest, 10 µM AZM ($\geq IC_{90}$) was used. Purified native MsrE protein was added at indicated concentrations. Results are means of three independent repeats with standard deviations shown by error bars. Uninhibited condition was used as a standard. (b) MsrE ribosome binding assay. *T. thermophilus* 70S ribosomes were pre-treated with AZM and incubated with native MsrE pre-treated with ATP (lane 1) or AMP-PNP (lane 2). For control assay, native MsrE in absence of ribosomes was used (lane 3). Lanes 4-7 show MsrE mutants E104Q/E413Q, R241A, H244A, and loop-truncated MsrE pre-incubated with ATP, respectively. Samples were pelleted through sucrose cushion and analysed by denaturing PAGE with SYPRO Ruby staining. Purified 70S ribosomes (lane 8) and native MsrE (lane 9) were mixed together at different ratios (lanes 10-14) in order to assess the stoichiometry of MsrE binding.

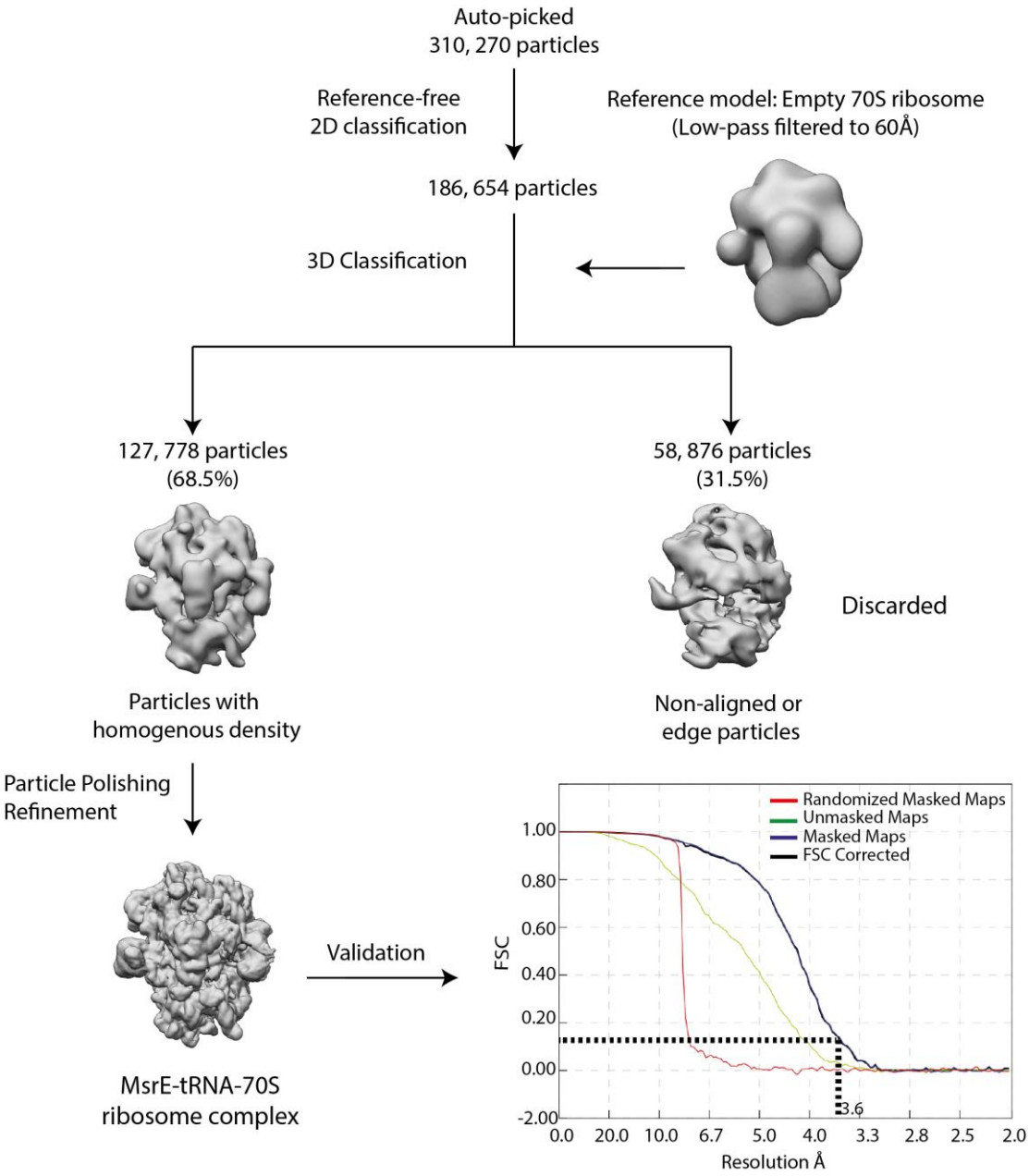

Figure S4. Cryo-EM data processing work-flow. After removal of non-aligning and edge particles, the remaining homogenous dataset yielded stoichiometric density for P-tRNA as well as MsrE. This population was further refined and validated with Fourier shell correlation (FSC) curves which estimated the resolution of the final reconstitution.

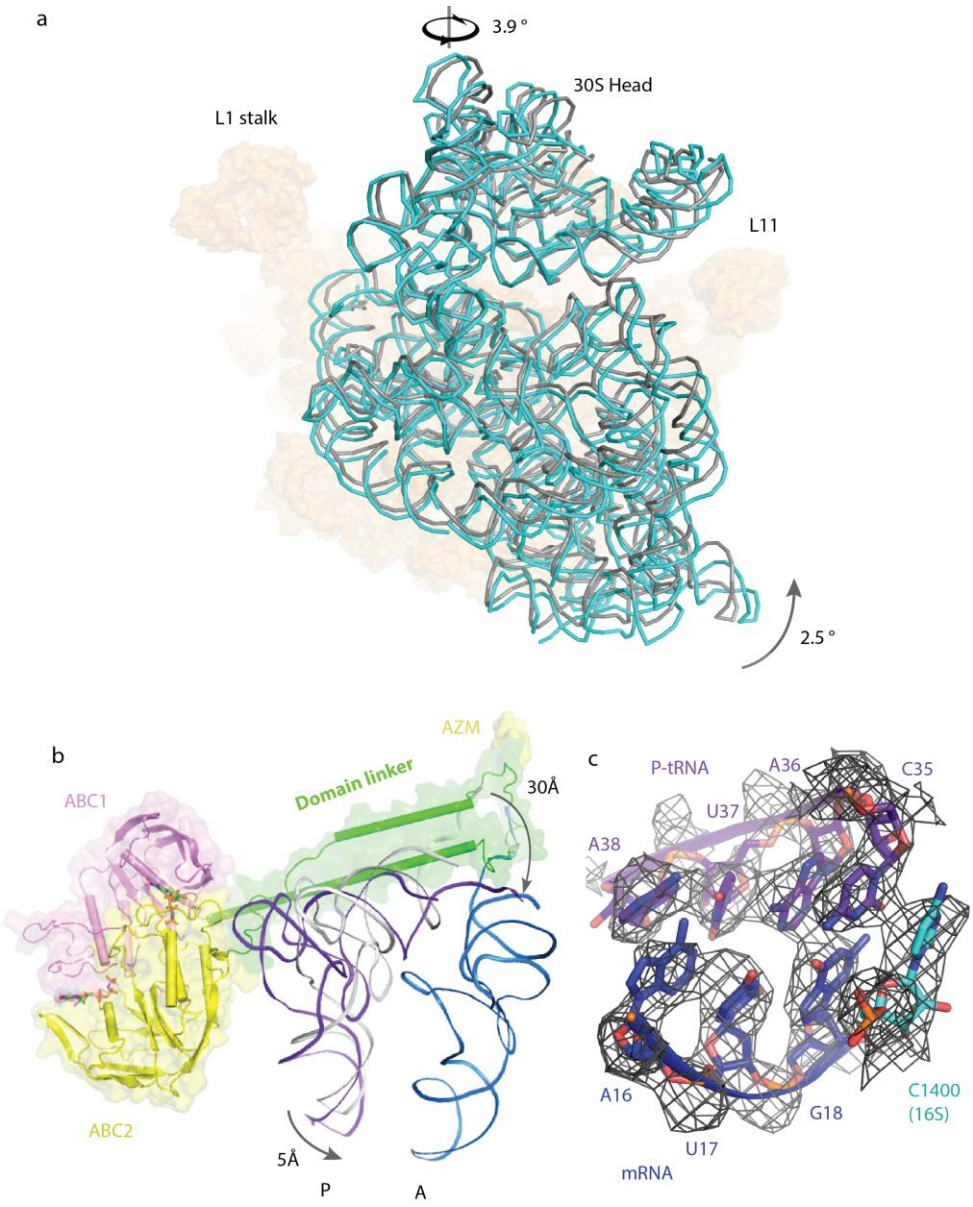

Figure S5. Conformational changes in ribosome upon MsrE binding. (a) 30S head swivel and body rotation with respect to 50S. For clarity, 16S rRNA (cyan) is shown in cartoon and 50S in surface (orange). For comparison, 16S rRNA of the post-peptidyl transfer ribosome (15) is shown (grey). Ribosomes are superimposed based on 23S rRNA. (b) Position of tRNA (purple) in MsrE-ribosome complex compared with P/P tRNA (grey) (15). For reference, MsrE and A/A tRNA (blue) (30) are shown as well. (c) P tRNA anticodon (purple) interaction with mRNA (dark blue). 16S rRNA residue C1400 is also shown.

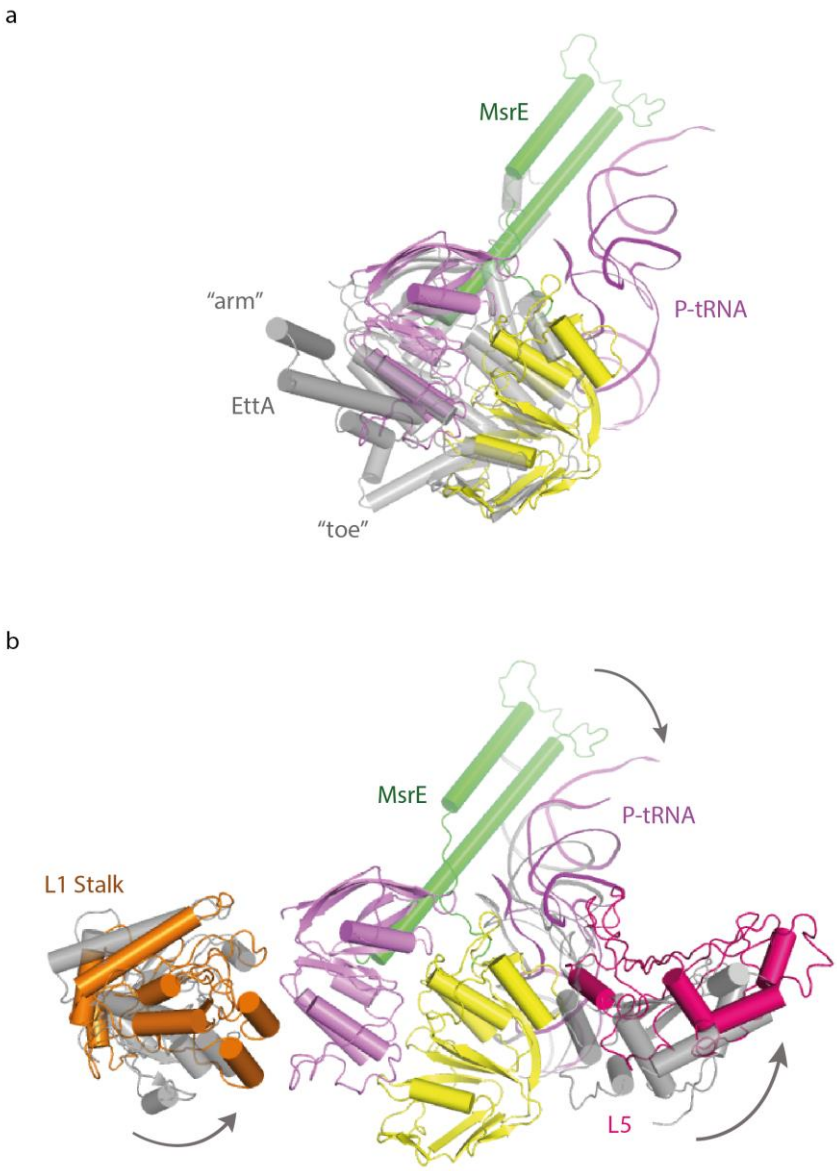

Figure S6. Comparison of the ribosome bound MsrE and EttA structures. (a) Superposition of ribosome bound MsrE and EttA (grey) (16) structures. EttA "arm" and "toe" regions are shown. (b) Comparison of the conformational changes in ribosome L1-stalk (orange) and L5 protein (hot pink) in MsrE-ribosome and EttA-ribosome (gray) (16) structures. P-site tRNA positions are shown also.

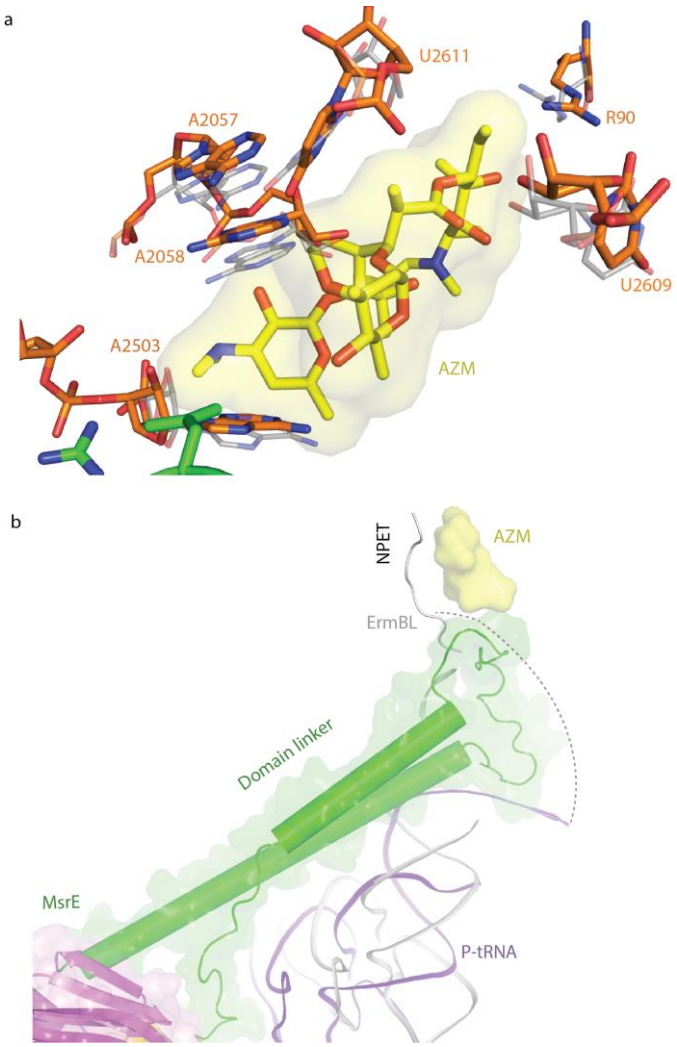

Figure S7. MsrE-ribosome complex AZM binding site and comparison with ErmBL leader peptide-induced ribosome-stalling complex. MsrE induced conformational changes in macrolide binding site (a). The orientation of key macrolide binding site residues in the MsrE-ribosome complex is compared with corresponding orientations (grey) in post-peptidyl transfer ribosome (15). For reference, AZM binding mode is shown based on alignment with the AZM-ribosome X-ray crystal structure (PDB ID: 4V7Y) (17). (b) MsrE-ribosome complex comparison with the ErmBL nascent chain-ribosome complex (PDB ID: 5JU8) (18). The dashed line shows the possible passageway for the nascent chain of the distorted P-tRNA upon MsrE binding given the available space and the structural flexibility around this area in the present complex.

Table S1

Effect of MsrE dose-dependent expression on AZM MIC of *E. coli* K12 MG1655 strain carrying pJN105-P$_{BAD}$-*msrE* plasmid

Arabinose (%)	AZM MIC (µg/ml)
6.4	512
3.2	512
1.6	512
0.8	256
0.4	256
0.2	128
0.1	64
0.05	32
0.025	32
0.012	16
0.006	8
0.003	8
0.0015	8
0.0000	8

Table S2

AZM MIC for *E. coli* MG1655 strain expressing mutant MsrE proteins

Plasmid	No induction	0.2% glucose	0.2% arabinose
pJN105	8	8	8
pJN105- **P_{BAD}** -*msrE*	8	8	128
pJN105- **P_{BAD}** -*ettA*	8	8	8
pJN105- **P_{BAD}** - pJN105- **P_{BAD}** *msrE*(E104Q/E413Q)	8	8	16
pJN105- **P_{BAD}** -*msrE*(E104Q)	8	8	64
pJN105- **P_{BAD}** -*msr*E(E413Q)	8	8	32
pJN105- **P_{BAD}** - *msrE*(R241A/H244A)	8	8	8
pJN105- **P_{BAD}** -*msrE*(R241A)	8	8	16
pJN105- **P_{BAD}** -*msrE*(L242A)	8	8	16
pJN105- **P_{BAD}** -*msrE*(L242G)	8	8	16
pJN105- **P_{BAD}** -*msrE*(H244A)	8	8	16
pJN105- **P_{BAD}** -*msrE*(Δloop)	8	8	8

Table S3

Cryo-EM data collection, refinement, and validation statistics

Data collection	
Particles	127,778
Pixel Size	1.11
Defocus range (μm)	-1.5 to -2.5
Voltage (kV)	300
Electron exposure (e–/Å^2)	50
Refinement	
Resolution (Å)	3.6
Map sharpening B-factor (Å^2)	-106
Average B-factor	194
FSC	0.143
Real-Space Correlation	
Mask CC	0.764
Volume CC	0.750
RMS Deviations	
Bond lengths (Å)	0.013
Bond angles (°)	1.472
Ramachandran plot	
Favored (%)	79.64
Allowed (%)	19.16
Outliers (%)	1.20

References

1. Liu H, Naismith JH (2008) An efficient one-step site-directed deletion, insertion, single and multiple-site plasmid mutagenesis protocol. *BMC Biotechnol* 8:91.
2. Selmer M *et al.* (2006) Structure of the 70S ribosome complexed with mRNA and tRNA. *Science* 313:1935–1942.
3. Kumar V *et al.* (2016) Structure of the GTP Form of Elongation Factor 4 (EF4) Bound to the Ribosome. *J Biol Chem* 291:12943–12950.
4. Suloway C *et al.* (2005) Automated molecular microscopy: the new Leginon system. *J Struct Biol* 151:41–60.
5. Brilot AF *et al.* (2012) Beam-induced motion of vitrified specimen on holey carbon film. *J Struct Biol* 177:630–637.
6. Rohou A, Grigorieff N (2015) CTFFIND4: Fast and accurate defocus estimation from electron micrographs. *J Struct Biol* 192:216–221.
7. Kimanius D, Forsberg BO, Scheres SHW, Lindahl E (2016) Accelerated cryo-EM structure determination with parallelisation using GPUs in RELION-2. *Elife* 5
8. Fernandez-Leiro R, Scheres SHW (2017) A pipeline approach to single-particle processing in RELION. *Acta Crystallogr D Struct Biol* 73:496–502.
9. Källberg M, Margaryan G, Wang S, Ma J, Xu J (2014) RaptorX server: a resource for template-based protein structure modeling. *Methods Mol Biol* 1137:17–27.
10. Pettersen EF *et al.* (2004) UCSF Chimera--a visualization system for exploratory research and analysis. *J Comput Chem* 25:1605–1612.
11. Emsley P, Lohkamp B, Scott WG, Cowtan K (2010) Features and development of Coot. *Acta Crystallogr D Biol Crystallogr* 66:486–501.

12. Adams PD et al (2010) PHENIX: a comprehensive Phyton-based system for macromolecular structure solution. *Acta Cryst* 66:213-221.
13. Kucukelbir A, Sigworth FJ, Tagare HD (2014) Quantifying the Local Resolution of Cryo-EM Density Maps. *Nature Methods* 11:63-65.
14. Boël G *et al.* (2014) The ABC-F protein EttA gates ribosome entry into the translation elongation cycle. *Nat Struct Mol Biol* 21:143–151.
15. Voorhees RM, Weixlbaumer A, Loakes D, Kelley AC, Ramakrishnan V (2009) Insights into substrate stabilization from snapshots of the peptidyl transferase center of the intact 70S ribosome. *Nat Struct Mol Biol* 16:528–533.
16. Chen B *et al.* (2014) EttA regulates translation by binding the ribosomal E site and restricting ribosome-tRNA dynamics. *Nat Struct Mol Biol* 21:152–159.
17. Bulkley D, Innis CA, Blaha G, Steitz TA (2010) Revisiting the structures of several antibiotics bound to the bacterial ribosome. *Proc Natl Acad Sci USA* 107:17158–17163.
18. Arenz S *et al.* (2016) A combined cryo-EM and molecular dynamics approach reveals the mechanism of ErmBL-mediated translation arrest. *Nat Commun* 7:12026.